Atmospheric
Chemistry
and Physics
Discussions

Open Access

Characteristics and formation mechanism of continuous extreme hazes in China: a case study in autumn of 2014 in the North China Plain

Y. R. Yang[1], X. G. Liu[1], Y. Qu[2], J. L. An[2], R. Jiang[3], Y. H. Zhang[4], Y. L. Sun[2], Z. J. Wu[4], F. Zhang[5], W. Q. Xu[2], and X. Q. Ma[6]

[1]State Key Laboratory of Water Environment Simulation, School of Environment, Beijing Normal University, Beijing 100875, China
[2]State Key Laboratory of Atmospheric Boundary Layer Physics and Atmospheric Chemistry, Institute of Atmospheric Physics, Chinese Academy of Sciences, Beijing 100029, China
[3]Shanghai Key Laboratory for Urban Ecological Processes and Eco-Restoration, School of Ecological and Environmental Sciences, East China Normal University, Shanghai 200241, China
[4]State Key Joint Laboratory of Environment Simulation and Pollution Control, College of Environmental Sciences and Engineering, Peking University, Beijing 100871, China
[5]College of Global Change and Earth System Science, Beijing Normal University, Beijing 100875, China

Discussion Paper | Discussion Paper | Discussion Paper | Discussion Paper

ACPD

15, 10987–11029, 2015

Characteristics and formation mechanism of continuous extreme hazes

Y. Yang et al.

Title Page

Abstract | Introduction

Conclusions | References

Tables | Figures

◄◄ | ►►

◄ | ►

Back | Close

Full Screen / Esc

Printer-friendly Version

Interactive Discussion

[6]Research Center for Eco-Environmental Sciences, Chinese Academy of Sciences, Beijing 100085, China

Correspondence to: X. G. Liu (liuxingang@bnu.edu.cn)
and Y. H. Zhang (yhzhang@pku.edu.cn)

Characteristics and formation mechanism of continuous extreme hazes

Y. Yang et al.

Title Page

Abstract	Introduction
Conclusions	References
Tables	Figures

|◄ ►|

◄ ►

Back Close

Full Screen / Esc

Printer-friendly Version

Interactive Discussion

Full Screen / Esc

Printer-friendly Version

Interactive Discussion

Abstract

Four extreme haze episodes occurred in October 2014 in the North China Plain (NCP). To clarify the formation mechanism of hazes in the autumn, strengthened observations were conducted in Beijing from 5 October to 2 November. The meteorological parameters, satellite data, chemical compositions and optical properties of aerosols were obtained. The hazes originated from NCP, developing in the southwest and northeast directions, with the highest concentration of $PM_{2.5}$ of 469 $\mu g\,m^{-3}$ in Beijing. NCP was dominated by a weak high pressure system during the haze episode, which resulted in low surface wind speed and relatively stagnant weather. Moreover, the wind slowed down around Beijing city. The secondary aerosols NO_3^- was always higher than that of SO_4^{2-}, which indicated the motor vehicles played a more important part in the hazes in October 2014, even though the oxidation rate from SO_2 to SO_4^{2-} was faster than that of NO_x to NO_3^-. Sudden increases of the concentrations of organic matter, Cl^- and BC (Black carbon) before each haze episode implied that regional transport of pollutants by biomass burning was important for haze formation during the autumn. A satellite map of fire points and the backward trajectories of the air masses also indicated this pollution source. The distinct decrease in the PBL (planetary boundary layer) height during four haze episodes restrained the vertical dispersion of the air pollutants. Water vapor also played a vital role in the formation of hazes by accelerating the chemical transformation of secondary pollutants, leading to hygroscopic growth of aerosols and altering the thermal balance of the atmosphere.

1 Introduction

Haze is an atmospheric phenomenon composed of smog, dust, and vapor suspended in air, with a horizontal visibility lower than 10 km and an RH lower than 90 % (Watson, 2002; Wu et al., 2007; Liu et al., 2013b). Haze events have attracted increased attention because of their close relationship with human diseases (Miller et al., 2007; Araujo

et al., 2008) and the alteration of the radiation budget in the atmosphere, leading to climate changes on Earth (Cahill, 1996; Jacobson, 2001).

In recent years, hazes have occurred frequently in China, especially in the North China Plain (NCP), which is one of the most populated and economically developed regions in China. Particulate matter is the primary pollutant during haze episodes; it occupies 85~90 % of the primary pollutants in most Chinese cities throughout the year (Wang et al., 2014). Three widespread and persistent haze episodes were recorded in China in January 2013 (Yang et al., 2015; Huang et al., 2014), October 2013 and February 2014. Two of these episodes seriously influenced the NCP (one in January 2013, and the other in February 2014), which were characterized by long durations, large regions of influence and high concentrations of $PM_{2.5}$ (particulate matter with an aerodynamic diameter equal or less than 2.5 μm) (Yang et al., 2015). The rapid increase in $PM_{2.5}$, which was seldom reported before, confused many researchers. Most studies explained that this phenomenon was due to the intense secondary formation (e.g., heterogeneous transform of SO_2 and NO_x to SO_4^{2-} and NO_3^-) (Liu et al., 2013a; Ji et al., 2014) and the huge regional transport of pollutants (Wang et al., 2014). In addition, stationary meteorological conditions and large local emission (e.g., coal combustion in winter) were also considered to be major factors leading to such severe hazes (Liu et al., 2013a; Sun et al., 2014).

Due to the heating supply in northern China during the winter (Ma et al., 2011) and the violent photoreaction during the summer (Wen et al., 2015), most studies concerning haze events in the NCP were performed in the winter and summer. Comparatively, haze formation in autumn has been investigated less often. Liu et al. (2013a) reported a case study on haze in September 2011 in Beijing and clarified that the key factors resulting in the formation and evolution of haze episodes were stable anti-cyclone synoptic conditions at the surface, the decreasing height of the PBL (planetary boundary layer), heavy pollution emissions from urban areas, the number and size evolution of aerosols, and hygroscopic growth for aerosol scattering. In Beijing city, the RH in autumn is high (Zhao et al., 2011), and biomass burning in the vicinity is prevalent due

Title Page

Abstract | Introduction

Conclusions | References

Tables | Figures

|◄ | ►|

◄ | ►

Back | Close

Full Screen / Esc

Printer-friendly Version

Interactive Discussion

CC BY

to autumn harvest (Wang et al., 2014). These special conditions may result in different formation mechanisms of haze in the autumn.

In October 2014, four serious haze events occurred, which were some of the severest hazes in NCP in the autumn period. The haze mainly influenced the NCP and Northeast China Region, covering an area of 560 000 km^2. The largest concentrations of PM$_{10}$ and PM$_{2.5}$ were 741 and 508 µg m^{-3}, which were recorded in Shijiazhuang, the capital of Hebei province. Until now, few studies have reported on this haze episode and its distinctive formation mechanism. In this study, comprehensive measurements were conducted from 5 October to 2 November in Beijing to investigate the characteristics and specific mechanism of continuous extreme hazes in the autumn.

2 Experiment

2.1 Experiment site

Beijing is the capital of the People's Republic of China and is the national center for politics, economics and culture. The GDP (gross domestic product) of Beijing in 2013 was USD 3.15 trillion with a growth rate of 7.7 %. The population of Beijing was 21.15 million with a population density of 1289 people km^{-2} at the end of 2013 (http://www.bjstats.gov.cn/nj/main/2014-tjnj/CH/index.htm). There are 5.4 million cars, with a growth of 0.237 million cars in Beijing as of 2013 (http://zhengwu.beijing.gov.cn/tjxx/tjgb/t1340447.htm). High population and economic levels have led to heavy emissions of air pollutants in Beijing.

Field measurements from 5 October to 2 January 2014 were performed at the urban atmospheric environment monitoring super-station (39.96° N, 116.36° E) on the campus of Beijing Normal University (BNU). This site is located at the northern part of Beijing. The third ring road, one of the main traffic lines of Beijing, is approximately 300 m to the north of the measurement site. The observation site was on the roof of a six-story building (approximately 20 m above ground level); all of the instruments

except the visibility sensor were installed in an air-conditioned room. Mass concentration of gases was measured by National Environmental Bureau on the Olympic Sports Center site (39.98° N, 116.39° E).

2.2 Measurement and method

The mass concentration of $PM_{2.5}$ was measured by TEOM (tapered element oscillating microbalance, RP1405F) at the BNU site, whereas the mass concentration of gases (SO_2, NO_2, CO and O_3) was monitored by the National Environmental Bureau, and the data were gathered from the Internet (http://www.pm25.in/). We choose the data from Olympic Sports Center site, since it was nearest to BNU site. Atmospheric visibility with range from 10 m to 80 km was measured by the visibility sensor (Belfort 6000) at the wavelength of 880 nm (Liu et al., 2013a), which consisted of a transmitter, a receiver, and a controller. The atmospheric extinction coefficient b_{ext} (RH) at 550 nm in units of inverse megameter (Mm^{-1}) is calculated by Eq. (1) from the visibility data (Koschmieder, 1924):

$$b_{ext}(RH) = \frac{3.912 \times 10^3}{Vis} \times \left(\frac{880}{550}\right) \tag{1}$$

The BC (black carbon) in $PM_{2.5}$ was measured using an Aethalometer (Model AE33, Magee Scientific Corporation) with seven wavelengths from 370 nm (UV) to 950 nm (IR) and a time resolution of 5 min. The aerosol absorption coefficient b_{ap} was calculated using Eq. (2):

$$b_{ap} = [BC] \times 6.6 \times \left(\frac{\lambda}{550}\right) \tag{2}$$

The aerosol scattering coefficient at dry condition, b_{sp} (dry), was measured by integrating a nephelometer (Model Aurora 3000, Ecotech, Australia) with a desiccant before the inlet.

Thus, the aerosol scattering coefficient under ambient condition b_{sp} (RH) was calculated using Eq.(3):

$$b_{sp}(\text{RH}) = b_{ext}(\text{RH}) - b_{ap} - b_{ag} - b_{sg} \tag{3}$$

Where b_{ag} is calculated using the experiential equation $b_{ag} = [\text{NO}_2] \times 0.33$ (Hodkinson, 1966) with the unit of NO_2 being ppbv, and the scattering coefficient by gas, b_{sg}, is assumed to be constant at a value of $10\,\text{Mm}^{-1}$ (Liu et al., 2008, 2013b).

The hygroscopic growth of aerosol scattering $f(\text{RH})$, is widely used as the ratio of the aerosol scattering coefficient under wet conditions to that under dry conditions. It is calculated using Eq. (4) (Liu et al., 2008):

$$f(\text{RH}) = \frac{b_{sp}(\text{RH})}{b_{sp}(\text{dry})} = \frac{b_{ext}(\text{RH}) - b_{ap} - b_{ag} - b_{sg}}{b_{sp}(\text{dry})} \tag{4}$$

The single scattering albedo (SSA) is the ratio of the aerosol scattering coefficient over the aerosol extinction coefficient at a given wavelength. In this study, SSA is calculated with $b_{sp}(\text{RH})$ and b_{ap} via Eq. (5):

$$\text{SSA} = \frac{b_{sp}(\text{RH})}{b_{sp}(\text{RH}) + b_{ap}} \tag{5}$$

The meteorological station (Vaisala, Finland) monitored solar radiation, wind direction, wind speed and relative humidity. The height of the PBL, the wind field graph and atmospheric back trajectories were obtained from the ARL (Air Resources Laboratory) at NOAA website (http://www.arl.noaa.gov/index.php). Meteorological data from the GDAS (Global Data Assimilation System) was used for the model calculation.

The NR-PM$_1$ (non-refractory submicron aerosol) species, including organics, SO_4^{2-}, NO_3^-, NH_4^+ and Cl^-, were measured in situ using an ACSM (aerosol chemical speciation monitor) with an air flow of $0.1\,\text{L min}^{-1}$ and a time resolution of 15 min. More detailed operations and calibrations of the ACSM can be found in the work of Sun et al. (2013). The instruments involved in this study are listed in Table 1.

Title Page

Abstract | Introduction

Conclusions | References

Tables | Figures

|◄ | ►|

◄ | ►

Back | Close

Full Screen / Esc

Printer-friendly Version

Interactive Discussion

3 Results and discussion

3.1 Characteristics of the haze episodes

3.1.1 Overall description

As illustrated in Fig. 2, there were four haze episodes during the field measurement in Beijing, which were 7 to 11 October, 17 to 20 October, 22 to 26 October, and 29 October to 1 November.

The highest concentration of $PM_{2.5}$ occurred at 18:00 LST on 25 October (the third episode), with a value of $469\,\mu g\,m^{-3}$. Although the haze was severe, the peak value was much lower than that ($900\,\mu g\,m^{-3}$) during the haze in January 2013 (Zhang et al., 2014). Before the peak, increasing $PM_{2.5}$ concentrations were observed. The four episodes had similar accumulation and dispersion patterns, in which the increasing slopes for the $PM_{2.5}$ values in four episodes resembled each other and the pollutants were dispersed in a few hours. The rates of increase of $PM_{2.5}$, which were represented by the slope of $PM_{2.5}$ concentrations, were calculated. To reduce the influence of the diurnal variation of $PM_{2.5}$, the first and last peak values in each haze episode were chosen in the calculation. Thus, the slope r is:

$$r\left(PM_{2.5},\ \mu g\,m^{-3}\,h^{-1}\right) = \frac{[PM_{2.5}]_{max} - [PM_{2.5}]_{min}}{T\,(h)} \tag{6}$$

The results are shown in Table 2.

In the four haze episodes, the rates of increase of the concentration of $PM_{2.5}$ were 4.03, 4.44, 4.16 and $2.00\,\mu g\,m^{-3}\,h^{-1}$. The first three hazes had similar rates of increase, and in the last haze episode, the concentration of $PM_{2.5}$ increased at half the rate of the other three hazes. Gaseous pollutants (SO_2, NO_2, CO, and O_3) also showed obvious increases during haze episodes, except for O_3 in the fourth episode (Fig. 3). Because a heat supply is unavailable in October in Beijing, the emission of SO_2, which is mainly from coal combustion, was much less than the emission of NO_2, which is mainly from

vehicle exhaust. The average mass concentration of NO_2 was 73.1 µg m^{-3}, which is much higher than that of SO_2 (9.8 µg m^{-3}). O_3 was a product of the photochemical reaction between nitrogen oxides (NO_x) and volatile organic compounds (VOCs). High concentrations of NO_2 resulted in a high concentration of O_3. However, O_3 remained
5 at a low level during the fourth episode, especially on 30 and 31 October, whereas PM$_{2.5}$ and other gaseous pollutants reached their peaks at this time, which indicated that the photochemical reaction during the fourth episode was not strong and that heterogeneous reactions play a major role in the haze formation in the fourth episode. All of the gaseous pollutants showed daily variation and reached a maximum on 18
10 October. These were also related to the variance in the height of the PBL, which will be discussed in Sect. 3.2.4.

Like the other severe hazes (Tao et al., 2014a, b) in last two years, the haze in October 2014 also influenced China to a large extent (Fig. 4). According to the PM$_{2.5}$ spatial distribution over China, the haze originated from the Northern China Plain (NCP) and
15 developed to the southwest and northeast directions. A similar situation occurred in September 2011, when the haze originated from Beijing and developed in the same directions (Liu et al., 2013a). Moreover, the haze influenced a large area of Middle China and Northeast China; for example, the concentration of PM$_{2.5}$ in Harbin, which is a large city in Northeast China, peaked at 664 µg m^{-3} during the third haze episode.

20 ## 3.1.2 Optical properties

The temporal variation of the aerosol scattering at ambient environment coefficient b_{sp} (RH), the absorption by NO_2 coefficient b_{ag}, the aerosol absorption coefficient b_{ap}, the atmospheric extinction at ambient environment coefficient b_{ext} (RH) and the SSA are shown in Fig. 5. Data for b_{ext} (RH) were complete for the whole observation period,
25 whereas the other three parameters were not available until 15 October. With clear diurnal variation, b_{sp}, b_{ap} and b_{ext} increased day by day during the haze episodes and decreased sharply at the end of these haze episodes. Because b_{sp} (RH) was calculated

using b_{ap} and b_{ext} and because b_{ap} was relatively small compared to b_{ext}, the b_{sp} (RH) had nearly the same temporal variation as b_{ext}. The maximum b_{ext} was 5611 Mm^{-1} at 22:00 LST on 25 October, and the average b_{ext} reached 1069 Mm^{-1}. Both data were much higher than those of other studies (Garland et al., 2008; Jung et al., 2009). The SSA in Fig. 5 was calculated using the aerosol extinction at ambient environment coefficient, b_{sp} (RH). Aerosol representing fresh emission always has a low SSA, whereas aged aerosol has a higher SSA (Garland et al., 2008). As a result, the SSA showed an increasing trend during the haze episodes. Four sudden decreases in the SSA were observed during the dawn of 16, 22, and 26 October and 1 November. The first two decreases occurred at the beginning of haze episodes, which represented large quantities of freshly emitted aerosol. Because local emissions in Beijing showed a steadier pattern, the sudden change in SSA indicated pollutant transport from the vicinity of Beijing (discussed in Sect. 3.2.2). The other two decreases occurred at the end of haze episodes when strong winds blew over Beijing and the pollutants were largely removed (discussed in Sect. 3.2.3). Aged aerosol was cleared and new aerosols increased in a short time (Guo et al., 2014). Thus, SSA decreased sharply.

3.2 Formation mechanism of haze episodes

3.2.1 Secondary transformation of aerosols

Water-soluble ions are a primary component of aerosols and play a major role in the hygroscopic growth of aerosols. The temporal variation of major components (organic matter, SO_4^{2-}, NO_3^-, NH_4^+, Cl^- and black carbon (BC)) in PM_1 is shown in Fig. 6. Organic matter contributed most to the PM_1, followed by NO_3^-, SO_4^{2-}, NH_4^+, BC and Cl^-. The mass concentration of SO_4^{2-} was always higher than that of NO_3^-, especially in the winter time, when the heat supply is prevalent in North China (Zhao et al., 2013). Although Beijing is replacing coal with natural gas for a heat supply, the influence from the vicinity is still enormous. However, in this study, the mass concentration of NO_3^-

was always higher than that of SO_4^{2-}. The concentration of NO_3^-, which was primarily transferred from NO_x, represented the contribution of motor vehicle sources. The heat supply is not available during October in NCP, and the motor vehicles remained at a similar level throughout the year, which implied that motor vehicles played a more important part in the hazes in the autumn. During the haze periods, the percentage of NO_3^- and NH_4^+ increased, whereas the percentage of organic matter continued to decrease. When strong wind blew pollutants away, the percentage of organic matter increased sharply. On the contrary, the percentage of NO_3^- decreased in a short time and did not return for a certain time. SO_4^{2-} varied similarly to NO_3^- but in a much milder pattern. After the strong wind, even the concentration of SO_4^{2-} decreased, and the return-back time was much shorter than that of NO_3^-. This indicates that even though the concentration of SO_4^{2-} was lower than that of NO_3^-, the oxidation rate from SO_2 to SO_4^{2-} was faster. It has been reported that the existence of high levels of NO_x may accelerate the reaction from SO_2 to SO_4^{2-} (He et al., 2014).

Even though all of the components in PM_1 increased during the haze events, the accumulation pattern might be different for each component. Comparatively, the increasing pattern of SNA (SO_4^{2-}, NO_3^- and NH_4^+) was likely from local emissions. Diurnal variation of the concentration of SNA also existed, but it was not as significant as that of organic matter, Cl^- and BC. There is also no sudden increase in the concentrations of SNA. They were more likely to accumulate stably with high RH and a stagnant atmosphere. When the RH was high and the atmosphere was stable, gases such as SO_2 and NO_x transform to SNA at a fast rate. A clear increase in the SNA percentage can be seen in the pie charts in Fig. 6. The values for SO_4^{2-}, NO_3^- and NH_4^+ in PM_1 increased from 8.48, 20.55 and 9.46 % in the non-haze period to 12.7, 27.5 and 12.14 % in the haze episode, respectively. Continuous increasing of SNA indicated that the formation of new SNA during the haze episodes contributes most of the formation of the haze. During the hazes in January 2013, high conversion from the gas phase of SO_2 and NO_x to the particle phase of SO_4^{2-} and NO_3^- was found, and heterogeneous forma-

Title Page

Abstract | Introduction

Conclusions | References

Tables | Figures

◄ | ►|

◄ | ►

Back | Close

Full Screen / Esc

Printer-friendly Version

Interactive Discussion

tion of SO_4^{2-} and NO_3^- was considered to be important, especially during low visibility episodes (Quan et al., 2014).

SOR and NOR were important factors, showing that gaseous species would be oxidized to secondary aerosols in the atmosphere (Sun et al., 2006). They are widely used in the analysis of the secondary transformation of aerosols. The temporal variations of SOR and NOR are shown in Fig. 7. SOR was mostly higher than 0.2, and NOR was mostly higher than 0.1, indicating intense secondary formation of SO_4^{2-} and NO_3^- (Fu et al., 2008). SOR and NOR increased during the haze episodes with accumulated pollutants. Furthermore, SOR increased more quickly than NOR. To compare the rate of increase of SOR and NOR, the slope of the SOR and NOR in the observed haze are calculated. To reduce the influence of the diurnal variation of SOR and NOR, the first and last peak values in the figure are chosen in the calculation. Thus, the slope r is:

$$r(\text{SOR, h}^{-1}) = \frac{\text{SOR}_{max} - \text{SOR}_{min}}{T(\text{h})} \tag{7}$$

$$r(\text{NOR, h}^{-1}) = \frac{\text{NOR}_{max} - \text{NOR}_{min}}{T(\text{h})} \tag{8}$$

The results are shown in Table 3.

In the three observed haze episodes, $r(\text{SOR})$ is 3.4, 1.6, and 4.2 times $r(\text{NOR})$, which indicated faster production of SO_4^{2-}, even though the concentration of SO_4^{2-} was lower than that of NO_3^-. Meanwhile, after the strong wind, which decreased SOR and NOR sharply, low SOR still existed, whereas NOR was nearly 0. These findings explained the shorter return time of SO_4^{2-} after the haze episodes.

3.2.2 Combustion of biomass and regional transport

Biomass burning became prevalent in NCP during the autumn harvest. The combustion was primarily conducted in the open field. Pollutants, such as BC and CO, were emitted on a large scale and influenced the air quality not only in the emission region but also

in the downstream city. Hence, biomass burning in the surrounding provinces was an important cause of the hazes in the autumn in Beijing. Fire points in China, based on data from MODIS Terra and Aqua satellites, on 6 October are shown in Fig. 8a. On 6 October, 267 fire points were found in China, among which 29, 163 and 30 fire points were found in Hebei, Henan and Shandong provinces, respectively. In total, 1957 fire points, which were caused by biomass burning in the whole of October, were found in China, among which 54, 26 and 57 fire points were found in Hebei, Henan and Shandong provinces, respectively. Although the fire points were more strictly controlled in 2014 compared to 2013, the influence of biomass burning still could not be neglected.

The backward trajectories of Beijing during the first haze episode reflect how the biomass burning influenced Beijing (Fig. 8b). A total of 9 backward trajectories of 48 h were drawn with the HYSPLIT model online version. The backward trajectories started from 17:00 LST on 11 October and restarted a new trajectory every 12 h. The air mass during the first haze episode mainly came from the south and southeast, originating from Hebei, Henan, Shandong and even Anhui Province. The pollutants from biomass burning in these provinces were transported to Beijing. Once the meteorological conditions were stagnant, haze formed and was aggravated in this region. A similar situation occurred in the haze in 2007 (Li et al., 2010). Therefore, biomass burning is a tough challenge for air pollution control in the autumn.

Based on the temporal variation of each component in Fig. 6, the organic matter, Cl^- and BC had similar variation patterns. In addition to clear diurnal variations, which were caused by the diurnal development of PBL, a sudden increase in the concentration before each haze period was found for the organic matter, Cl^- and BC. On 18 October, the height of the PBL (468.7 m) was 21.1 % higher than that on 17 October (386.9 m), but the concentrations of organic matter, Cl^- and BC were 6, 6 and 4 times the values of the day before. Organic matter, Cl^- and BC were emitted from biomass burning; abnormal high values and a sudden increase in organic matter, Cl^- and BC indicated spatial transport of pollutants from straw burning. Consequently, regional pol-

Title Page

Abstract | Introduction

Conclusions | References

Tables | Figures

|◄ | ►|

◄ | ►

Back | Close

Full Screen / Esc

Printer-friendly Version

Interactive Discussion

lutant transport was important for haze formation in October 2014, and straw burning was a significant pollution source.

3.2.3 Stationary synoptic condition

Pressure systems can influence the wind and precipitation of a region. Surface weather maps of East Asia at 02:00 LST on 7~10 October during the first haze episode are shown in Fig. 9. The NCP was dominated by a weak high-pressure system on 7 October, which lasted for the next two days. The weak high-pressure system resulted in low surface wind and relatively stagnant weather, which was unfavorable for the dispersion of air pollutants. The high-pressure system slowly moved towards the northeast. Meanwhile, the Mongolia anticyclone (a low-pressure system) moved towards and encountered the high-pressure system on 9 October, which brought wind and caused a small decrease in $PM_{2.5}$ on the dawn of 9 October. However, the weak high-pressure system dominated the NCP on 10 October, and the weather became stagnant again until 11 October, when another strong Mongolia anticyclone moved to the NCP, and the first haze episode ended.

The wind fields at 02:00 LST on 10, 20, 24, and 31 October in the NCP region are shown in Fig. 10, representing typical days in the four haze episodes. Generally, the wind speeds are slow during the haze episodes. In addition, the wind slowed sharply around Beijing city in all four figures. For example, on 31 October, the wind over the NCP came east from the Bohai Sea. The wind separated into two directions when it encountered Beijing, one blowing to the north and the other blowing to the south. The wind over Beijing maintained a low speed. A similar phenomenon was observed in January 2013 when a severe haze occurred in Beijing (Tao et al., 2014b). Moreover, the wind on 10 October was smooth, blowing from the southeast of Beijing and then turning to the northeast. The wind around Beijing was clearly slowed and became strong after blowing over Beijing. The city acted as a large obstacle for the wind, slowing the wind speed, disturbing the wind direction and affecting other properties of the wind (Miao et al., 2009). The wind on 20 October was more complex. Winds from the southwest

and northwest blew toward and converged at Beijing. The winds from the two directions weakened each other, creating stagnant conditions in Beijing. The pollutants in the vicinity were brought to Beijing, accumulating and reacting further (Zhao et al., 2013). On 24 October, the wind was similar to that on 10 October, with the exception of the disordered directions around Beijing city.

The wind rose diagram overlaid with the $PM_{2.5}$ concentrations from 5 October to 2 November are shown in Fig. 11. The winds blew mainly from three directions: northwest, northeast, and southwest. In each direction, the higher the wind speeds were, the lower the $PM_{2.5}$ concentrations were. The average wind speed was $1.1\,\mathrm{m\,s^{-1}}$, which was slightly higher than that ($0.9\,\mathrm{m\,s^{-1}}$) in September 2011, when another haze episode occurred (Liu et al., 2013a). Furthermore, the $PM_{2.5}$ concentrations were relatively high within the wind speed limit: $1\,\mathrm{m\,s^{-1}}$ for wind from the northwest, $1.5\,\mathrm{m\,s^{-1}}$ for wind from the northeast and $3\,\mathrm{m\,s^{-1}}$ for wind from the southwest. For example, when the wind was from the northeast and the wind speed was lower than $1.5\,\mathrm{m\,s^{-1}}$, nearly all of the $PM_{2.5}$ concentrations exceeded $75\,\mathrm{\mu g\,m^{-3}}$ (the national secondary standard of $PM_{2.5}$) and vice versa. Nevertheless, when the wind blew northwest, with wind directions concentrating between 270° to 315°, the wind speed limit decreased to $1\,\mathrm{m\,s^{-1}}$. Thus, with similar wind speeds, the concentration of $PM_{2.5}$ was lower. Zhang et al. (2015) made a research on relationships of evolution of $PM_{2.5}$ concentrations and meteorological conditions. In Beijing city, winds from northeast and southwest will results in higher concentration of $PM_{2.5}$ and winds from northeast will leads to lowest concentration of $PM_{2.5}$ in autumn and winter. It could also be clearly found in the haze during January 2013 in Beijing (Yang et al., 2015). However, winds in January 2013 distributed more equally in every direction while winds in October 2014 concentrated in specific direction. Differences between every wind direction were less in January 2013. High concentration (over $75\,\mathrm{\mu g\,m^{-3}}$) of $PM_{2.5}$ can also be found at wind speeds over $2\,\mathrm{m\,s^{-1}}$ when blowing northwest.

3.2.4   Variance of the PBL height

The development of the PBL, which is mainly influenced by air temperature and dynamics, affects the vertical dispersion of pollutants. When the PBL height is low, the pollutants stay at the surface layer and maintain a higher level. This can easily lead to
5   haze formation on the ground.

As depicted in Fig. 12, the heights of the PBL between the two haze episodes were relatively high, and a distinct descent of the PBL height was found during the four haze episodes. The lowest PBL at noon was 384 m on 17 October. It was only 14 % of the PBL height before the haze (2718 m on 15 October). Because it is difficult to
10   break through the PBL, the local pollutants were compressed and accumulated near the surface, leading to a high concentration of $PM_{2.5}$. This is not similar to cases reported in other haze episodes (Yang et al., 2015). The temperature during each haze episode in October 2014 maintained a constant level or even increased (Fig. 2). Normally, a higher temperature, which will enhance the PBL development, is conducive to
15   higher PBL. However, the formation of hazes in October 2014 was influenced by many factors. The dynamics of the atmosphere are another important factor from the local perspective. The deficiency of horizontal movement of the atmosphere affects the vertical development of the PBL. The highest PBL occurred on 16 October, when a cold and fast wind blew over Beijing. The cold and fast air mass from Mongolia is an ef-
20   fective removal mechanism of the haze not only in the horizontal direction but also in the vertical direction. Once the cold air from the northwest blows over the NCP, it not only promotes the horizontal dispersion of pollutants but also accelerates the vertical diffusion of pollutants because the height of the PBL is rapidly increased.

3.2.5   Impact of the relative humidity on haze

25   Four haze episodes in October 2014 were characterized by higher RH. The RH was over 90 % during the severest haze period, and it sometimes reached 100 % in October 2014. The high RH aggravated the haze.

Characteristics and formation mechanism of continuous extreme hazes

Y. Yang et al.

The relationships between RH and SOR and between RH and NOR are illustrated in Fig. 13. SOR and NOR were highly correlated with RH. The correlation coefficients of SOR and NOR with RH are 0.79 and 0.55, respectively, which are much higher than those in a previous study (Han et al., 2014), indicating the particularly high impor-

5   tance of RH during the haze episodes in this study. SOR reached a minimum when RH was approximately 40 %. When RH was > 40 %, SOR increased with increasing RH, whereas SOR decreased with increasing RH when RH was < 40 %. The conversion from SO_2 to SO_4^{2-} requires water vapor as a reactant. Hence, when RH was > 40 %, the high RH became a major factor accelerating the production of SO_4^{2-}. The conver-

10   sion is an endothermic reaction, which indicates that high temperature can promote the conversion. RH and temperature have an inverse correlation. When the RH was lower than 40 %, water was not adequate to accelerate the conversion. As a result, the temperature became the most important factor in the reaction. Therefore, when the RH was lower than 40 %, SOR decreased with decreasing temperature but not with

15   increasing RH. The formation of NO_3^- is more complex than that of SO_4^{2-}, so the correlation of NOR and RH was much weaker than that of SOR and RH. However, a clear positive correlation was still observed. No minimum value was found for NOR, and high RH can promote NOR.

The measured $f(RH)$ values at ambient RH during the observed period are depicted

20   in Fig. 14. The curve is similar to those of other studies, indicating an increasing tendency of $f(RH)$ with increasing RH. Usually, the exponential relationship between $f(RH)$ and RH can be fitted by an empirical function: $f(RH) = 1 + a(RH/100)^b$. In this study, the curve fitting parameters a and b were 3.79 and 6.10, respectively. $f(RH)$ values at an RH of 80 %, which had an average value of 1.97 in this study, are extracted for com-

25   parison with other studies. When the RH was 80 %, the aerosol particulate scattering coefficient was nearly 2 times that in dry conditions, which is relatively large compared with other studies (Liu et al., 2013b). Consequently, the RH contributed much more to aerosol extinctions in October 2014, leading to more severe hazes.

Visibility dependences on the mass concentration of $PM_{2.5}$ at different RH intervals are shown in Fig. 15 overall, the visibility decreased rapidly with increasing $PM_{2.5}$ concentrations. In addition, with increasing RH, the visibility decreased faster. For example, when the RH was less than 30 % and the mass concentration of $PM_{2.5}$ was lower than 85 µg m^{-3}, all of the visibilities were over 10 km. However, when the RH was greater than 90 %, no visibility was more than 10 km in this observation. To quantify the relationship between visibility, the $PM_{2.5}$ concentration and RH, Eq. (8) is used:

$$b_{ext}(RH) = b_{sp}(RH) + b_{ap} + b_{sg} + b_{ag}$$

$$= Q_{SP} \times PM_{2.5} \times \left(1 + a \times \left(\frac{RH}{100}\right)^b\right) + Q_{ap} \times PM_{2.5} + 34 \qquad (9)$$

Where Q_{sp} and Q_{ap} are the mass scattering and absorbing efficiency, which are the ratios of b_{sp} and b_{ap} to $PM_{2.5}$, respectively. The average values of Q_{sp} and Q_{ap} in this study are $3.10\,m^2\,g^{-1}$ and $0.42\,m^2\,g^{-1}$. Curves of the dependence of visibility on the $PM_{2.5}$ concentration at different RH intervals are shown in Fig. 15. The calculated curves showed the same trend as the dotted figure: the higher the RH was, the faster the visibility decreased as the concentration of $PM_{2.5}$ increased. When the concentration of $PM_{2.5}$ reached $75\,\mu g\,m^{-3}$ (the national secondary standard of $PM_{2.5}$), the visibility surpassed 10 km only when the RH was lower than 60 %. To control haze, keeping $PM_{2.5}$ under the national second standard alone is sufficient.

In previous studies, a temperature decrease was often reported (Liu et al., 2013a). It not only deprived the dynamics of the PBL development but also resulted in less heat turbulence, which is unfavorable for pollutant dispersion. Moreover, negative aerosol radiation forcing (ARF) was always recorded, indicating the feedback mechanism between radiation and aerosol loading (Quan et al., 2014). However, in this study, even though the solar radiation was reduced during the haze episodes, the temperature was steady or even increasing over a longer temporal range (several days). Water vapor, a greenhouse gas, had a vital effect on the atmospheric thermal balance. The short-

Title Page

Abstract   Introduction

Conclusions   References

Tables   Figures

◀   ▶

◀   ▶

Back   Close

Full Screen / Esc

Printer-friendly Version

Interactive Discussion

wave radiation from the sun is not absorbed by water vapor, but the long-wave radiation from the earth can be largely absorbed by it. As a result, even less solar radiation reached the earth's surface, and the radiation from the earth supplied increasing heat to the atmosphere with increasing RH. Increasing temperature accelerated the chemical reaction rate of aerosols and aggravated the haze. This situation could also be found in the haze in January 2013, but little research has focused on the temperature variation. Figure 16 depicts how RH influenced the haze formation. Water vapor in the atmosphere played a vital role in the formation of haze, which can not only accelerate the chemical transformation of secondary pollutants but also lead to hygroscopic growth of aerosols. Furthermore, as an important greenhouse gas, it absorbed surface radiation, altering the thermal balance of the atmosphere, which finally affected haze formation. RH in autumn is much higher than winter (Dong et al., 2013). It highly increases the rate of secondary reaction and hygroscopic growth. Thus, when only considering RH, with the same level of emission haze in autumn will be severer. However, in reality larger quantity of emission and increasing RH in last decade in winter (Cheng et al., 2015) resulted in heavier haze in winter season.

4   Conclusions

Comprehensive measurements were conducted during the haze episode from 5 October to 2 November 2014. To clarify the formation mechanism of haze in Beijing, the physical and chemical characteristics of aerosol and the relevant meteorology parameters were analyzed. The major conclusions are as follows:

1. Four distinct haze episodes occurred in October 2014 in Beijing, China. The highest concentration of $PM_{2.5}$ was $469\,\mu g\,m^{-3}$ in Beijing, and the highest increasing rate of the concentration of $PM_{2.5}$ was $4.44\,\mu g\,m^{-3}\,h^{-1}$. The haze originated from the Northern China Plain (NCP), developing to the southwest and northeast directions.

2. The concentration of SO_4^{2-} was lower than that of NO_3^-, but the oxidation rate of SO_2 to SO_4^{2-} was faster than that of NO_2 to NO_3^-. Sharp increases in the SNA fraction in PM_1 in the haze episode indicated that new formation of SNA contributed most to the formation of haze.

3. In total, 54, 26 and 57 fire points were found in Hebei, Henan and Shandong provinces, respectively. The air mass during the first haze episodes mainly came from the south and southeast, originating from these provinces. The sudden increase in the concentration of organic matter, Cl^- and BC before each haze period indicated the importance of biomass burning and transport in the haze formation in October 2014.

4. NCP was dominated by a weak high-pressure system during haze episodes. Beijing city slowed the wind speed and disturbed the wind direction. Overall, the winds blew from the northwest, northeast, and southwest. The $PM_{2.5}$ concentrations were relatively high within the wind speed boundary: $1\,\mathrm{m\,s}^{-1}$ for wind from the northwest, $1.5\,\mathrm{m\,s}^{-1}$ for wind from the northeast and $3\,\mathrm{m\,s}^{-1}$ for wind from the southwest.

5. A distinct decrease in the PBL height was observed during the four haze periods, compressing the local pollutants closer to the surface.

6. The four haze episodes in October 2014 were characterized by higher RH. High RH influenced the haze formation in three ways: accelerating the chemical transformation of secondary pollutants, leading to hygroscopic growth of aerosols and altering the thermal balance of the atmosphere.

References

Araujo, J. A., Barajas, B., Kleinman, M., Wang, X., Bennett, B. J., Gong, K. W., Navab, M., Harkema, J., Sioutas, C., Lusis, A. J., and Nel, A. E.: Ambient particulate pollutants in the ultrafine range promote early atherosclerosis and systemic oxidative stress, Circ. Res., 102, 589–596, 2008.

Cahill, T. A.: Climate forcing by anthropogenic aerosols: the role for PIXE, Nucl. Instrum. Meth. B, 109, 402–406, 1996.

Cheng, Y., He, K. B., Du, Z. Y., Zheng, M., Duan, F. K., and Ma, Y. L.: Humidity plays an important role in the $PM_{2.5}$ pollution in Beijing, Environ. Pollut., 197, 68–95, 2015.

Dong, X. L., Liu, D. M., and Gao, S. P.: Seasonal variations of atmospheric heterocyclic aromatic amines in Beijing, China, Atmos. Res., 120–121, 287–297, 2013.

Fu, Q., Zhuang, G., Wang, J., Xu, C., Huang, K., Li, J., Hou, B., Lu, T., and Streets, D. G.: Mechanism of formation of the heaviest pollution episode ever recorded in the Yangtze River Delta, China, Atmos. Environ., 42, 2023–2036, 2008.

Garland, R. M., Yang, H., Schmid, O., Rose, D., Nowak, A., Achtert, P., Wiedensohler, A., Takegawa, N., Kita, K., Miyazaki, Y., Kondo, Y., Hu, M., Shao, M., Zeng, L. M., Zhang, Y. H., Andreae, M. O., and Pöschl, U.: Aerosol optical properties in a rural environment near the mega-city Guangzhou, China: implications for regional air pollution, radiative forcing and remote sensing, Atmos. Chem. Phys., 8, 5161–5186, doi:10.5194/acp-8-5161-2008, 2008.

Guo, S., Hu, M., Zamora, M. L., Peng, J., Shang, D., Zheng, J., Du, Z., Wu, Z., Shao, M., Zeng, L., Molina, M. J., and Zhang, R.: Elucidating severe urban haze formation in China, P. Natl. Acad. Sci. USA, 111, 17373–17378, 2014.

Han, T., Liu, X., Zhang, Y., Qu, Y., Gu, J., Ma, Q., Lu, K., Tian, H., Chen, J., Zeng, L., Hu, M., and Zhu, T.: Characteristics of aerosol optical properties and their chemical apportionments during CAREBeijing 2006, Aerosol Air Qual. Res., 14, 1431–1442, 2014.

He, H., Wang, Y., Ma, Q., Ma, J., Chu, B., Ji, D., Tang, G., Liu, C., Zhang, H., and Hao, J.: Mineral dust and NO_x promote the conversion of SO_2 to sulfate in heavy pollution days, Sci. Rep., 4, 4172, doi:10.1038/srep04172, 2014.

Hodkinson, J. R.: Calculation of colour and visibility in urban atmospheres polluted by gaseous NO_2, Air Water Pollut., 10, 137–144, 1966.

Huang, K., Zhuang, G., Wang, Q., Fu, J. S., Lin, Y., Liu, T., Han, L., and Deng, C.: Extreme haze pollution in Beijing during January 2013: chemical characteristics, formation mechanism and

Characteristics and formation mechanism of continuous extreme hazes

Y. Yang et al.

Title Page

Abstract | Introduction

Conclusions | References

Tables | Figures

◀ | ▶

◀ | ▶

Back | Close

Full Screen / Esc

Printer-friendly Version

Interactive Discussion

role of fog processing, Atmos. Chem. Phys. Discuss., 14, 7517–7556, doi:10.5194/acpd-14-7517-2014, 2014.

Jacobson, M. Z.: Strong radiative heating due to the mixing state of black carbon in atmospheric aerosols, Nature, 409, 695–697, 2001.

Ji, D., Li, L., Wang, Y., Zhang, J., Cheng, M., Sun, Y., Liu, Z., Wang, L., Tang, G., Hu, B., Chao, N., Wen, T., and Miao, H.: The heaviest particulate air-pollution episodes occurred in northern China in January, 2013: insights gained from observation, Atmos. Environ., 92, 546–556, 2014.

Jung, J., Lee, H., Kim, Y. J., Liu, X., Zhang, Y., Gu, J., and Fan, S.: Aerosol chemistry and the effect of aerosol water content on visibility impairment and radiative forcing in Guangzhou during the 2006 Pearl River Delta campaign, J. Environ. Manage., 90, 3231–3244, 2009.

Koschmieder, H.: Theorie der horizontalen Sichtweite, Beitr. Phys. frei. Atmos., 12, 33–53, 1924.

Li, W. J., Shao, L. Y., and Buseck, P. R.: Haze types in Beijing and the influence of agricultural biomass burning, Atmos. Chem. Phys., 10, 8119–8130, doi:10.5194/acp-10-8119-2010, 2010.

Liu, X. G., Cheng, Y. F., Zhang, Y. H., Jung, J. S., Sugimoto, N., Chang, S. Y., Kim. Y. J., Fan, S. J., and Zeng, L. M.: Influences of relative humidity and particle chemical composition on aerosol scattering properties during the 2006 PRD campaign, Atmos. Environ., 42, 1525–1536, 2008.

Liu, X. G., Li, J., Qu, Y., Han, T., Hou, L., Gu, J., Chen, C., Yang, Y., Liu, X., Yang, T., Zhang, Y., Tian, H., and Hu, M.: Formation and evolution mechanism of regional haze: a case study in the megacity Beijing, China, Atmos. Chem. Phys., 13, 4501–4514, doi:10.5194/acp-13-4501-2013, 2013a.

Liu, X. G., Gu, J. W., Li, Y. P., Cheng, Y. F., Qu, Y., Han, T. T., Wang, J. L., Tian, H. Z., Chen, J., and Zhang, Y. H.: Increase of aerosol scattering by hygroscopic growth: observation, modeling, and implications on visibility, Atmos. Res., 132–133, 91–101, 2013b.

Ma, N., Zhao, C. S., Nowak, A., Müller, T., Pfeifer, S., Cheng, Y. F., Deng, Z.Z., Liu, P. F., Xu, W. Y., Ran, L., Yan, P., Göbel, T., Hallbauer, E., Mildenberger, K., Henning, S., Yu, J., Chen, L. L., Zhou, X. J., Stratmann, F., and Wiedensohler, A.: Aerosol optical properties in the North China Plain during HaChi campaign: an in-situ optical closure study, Atmos. Chem. Phys., 11, 5959–5973, doi:10.5194/acp-11-5959-2011, 2011.

Title Page

Abstract | Introduction

Conclusions | References

Tables | Figures

◀ | ▶

◀ | ▶

Back | Close

Full Screen / Esc

Printer-friendly Version

Interactive Discussion

Miao, S., Chen, F., LeMone, M. A., Tewari, M., Li, Q., and Wang, Y.: An observational and modeling study of characteristics of urban heat island and boundary layer structures in Beijing, J. Appl. Meteorol. Clim., 48, 484–501, 2009.

Miller, K. A., Siscovick, D. S., Sheppard, L., Shepherd, K., Sullivan, J. H., Anderson, G. L., and Kaufman, J. D.: Long-term exposure to air pollution and incidence of cardiovascular events in women, New Engl. J. Med., 356, 447–458, 2007.

Quan, J., Tie, X., Zhang, Q., Liu, Q., Li, X., Gao, Y., and Zhao, D.: Characteristics of heavy aerosol pollution during the 2012–2013 winter in Beijing, China, Atmos. Environ., 88, 83–89, 2014.

Sun, Y. L., Zhuang, G. S., Tang, A. H., Wang, Y., and An, Z. S.: Chemical characteristics of PM2. 5 and PM10 in haze-fog episodes in Beijing, Environ. Sci. Technol., 40, 3148–3155, 2006.

Sun, Y. L., Wang, Z. F., Fu, P. Q., Yang, T., Jiang, Q., Dong, H. B., Li, J., and Jia, J. J.: Aerosol composition, sources and processes during wintertime in Beijing, China, Atmos. Chem. Phys., 13, 4577–4592, doi:10.5194/acp-13-4577-2013, 2013.

Sun, Y. L., Jiang, Q., Wang, Z. F., Fu, P. Q., Li, J., Yang, T., and Yin, Y.: Investigation of the sources and evolution processes of severe haze pollution in Beijing in January 2013, J. Geophys. Res.-Atmos., 119, 4380–4398, 2014.

Tao, M., Chen, L., Wang, Z., Ma, P., Tao, J., and Jia, S.: A study of urban pollution and haze clouds over northern China during the dusty season based on satellite and surface observations, Atmos. Environ., 82, 183–192, 2014a.

Tao, M., Chen, L., Xiong, X., Zhang, M., Ma, P., Tao, J., and Wang, Z.: Formation process of the widespread extreme haze pollution over northern China in January 2013: implications for regional air quality and climate, Atmos. Environ., 98, 417–425, 2014b.

Wang, H., Xu, J., Zhang, M., Yang, Y., Shen, X., Wang, Y., Chen, D., and Guo, J.: A study of the meteorological causes of a prolonged and severe haze episode in January 2013 over central-eastern China, Atmos. Environ., 98, 146–157, 2014.

Wang, W., Maenhaut, W., Yang, W., Liu, X., Bai, Z., Zhang, T., Claeys, M., Cachier, H., Dong, S., and Wang, Y.: One-year aerosol characterization study for $PM_{2.5}$ and PM_{10} in Beijing, Atmos. Pollut. Res., 5, 554, doi:10.5094/APR.2014.064, 2014.

Watson, J. G.: Visibility: science and regulation, J. Air Waste Manage., 52, 628–713, 2002.

Wen, L., Chen, J. M., Yang, L. X., Wang, X. F., Xu, C. H., Sui, X., Yao, L., Zhu, Y. H., Zhuang, J. M., Zhu, T., and Wang, W. X.: Enhanced formation of fine particulate nitrate at a rural site

on the North China Plain in summer: The important roles of ammonia and ozone, Atmos. Environ., 101, 294–302, 2015.

Wu, D., Bi, X., Deng, X., Li, F., Tan, H., Liao, G., and Huang, J.: Effect of atmospheric haze on the deterioration of visibility over the Pearl River Delta, Acta Meteorol. Sin., 21, 215–223, 2007.

Xue, J., Griffith, S. M., Yu, X., Lau, A. K. H., and Yu, J. Z.: Effect of nitrate and sulfate relative abundance in $PM_{2.5}$ on liquid water content explored through half-hourly observations of inorganic soluble aerosols at a polluted receptor site, Atmos. Environ., 99, 24–31, 2014.

Yang, Y., Liu, X., Qu, Y., Wang, J., An, J., Zhang, Y., and Zhang, F.: Formation mechanism of continuous extreme haze episodes in the megacity Beijing, China, in January 2013, Atmos. Res., 155, 192–203, 2015.

Zhang, J. K., Sun, Y., Liu, Z. R., Ji, D. S., Hu, B., Liu, Q., and Wang, Y. S.: Characterization of submicron aerosols during a month of serious pollution in Beijing, 2013, Atmos. Chem. Phys., 14, 2887–2903, doi:10.5194/acp-14-2887-2014, 2014.

Zhang, Z. Y., Zhang, X. L., Gong, D. Y., Quan, W. J., Zhao, X. J., Ma, Z. Q., and Kim, S. J.: Evolution of surface O_3 and $PM_{2.5}$ concentrations and their relationships with meteorological conditions over the last decade in Beijing, Atmos. Environ., 108, 67–75, 2015.

Zhao, P., Zhao, X., Zhang, X., and Xu, X.: Long-term visibility trends and characteristics in the region of Beijing, Tianjin, and Hebei, China, Atmos. Res., 101, 711–718, 2011.

Zhao, X. J., Zhao, P. S., Xu, J., Meng„ W., Pu, W. W., Dong, F., He, D., and Shi, Q. F.: Analysis of a winter regional haze event and its formation mechanism in the North China Plain, Atmos. Chem. Phys., 13, 5685–5696, doi:10.5194/acp-13-5685-2013, 2013.

Title Page

Abstract | Introduction

Conclusions | References

Tables | Figures

|◀ | ▶|

◀ | ▶

Back | Close

Full Screen / Esc

Printer-friendly Version

Interactive Discussion

Table 1. Overview of the instruments involved in this study.

Instrument	Parameter	Manufacturer model
TEOM	$PM_{2.5}$	Thermo. Electron., RP1405F
Visibility meter	Visibility	Belfort 6000
Aethalometer	BC	AE33
Integrating nephelometer	Aerosol scattering coefficient	Ecotech, Aurora 3000
Wind speed/Temperature/RH sensor	Wind speed, Temperature, RH	Vaisala, GMT220, HMP45
ACSM	The NR-PM_1 species	/

Table 2. The slopes of $PM_{2.5}$ concentrations during the four haze episodes ($\mu g\,m^{-3}\,h^{-1}$).

	Episode 1 ($\mu g\,m^{-3}\,h^{-1}$)	Episode 2 ($\mu g\,m^{-3}\,h^{-1}$)	Episode 3 ($\mu g\,m^{-3}\,h^{-1}$)	Episode 4 ($\mu g\,m^{-3}\,h^{-1}$)
$r(PM_{2.5})$	4.03	4.44	4.16	2.00

Table 3. The slopes of SOR and NOR during three haze episodes.

	Episode 2 (h^{-1})	Episode 3 (h^{-1})	Episode 4 (h^{-1})
$r(\text{SOR})$	5.63×10^{-3}	7.05×10^{-3}	6.22×10^{-3}
$r(\text{NOR})$	1.64×10^{-3}	4.5×10^{-3}	1.49×10^{-3}
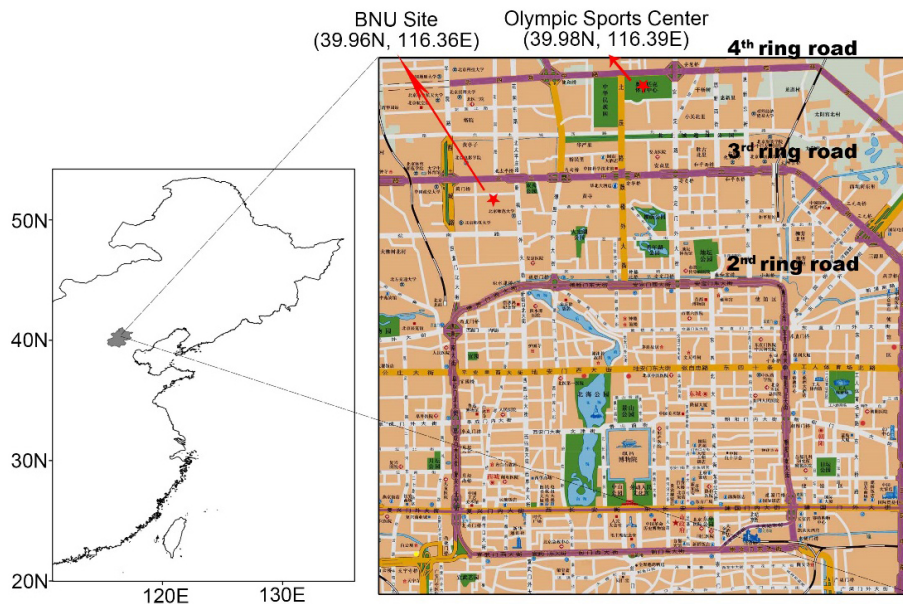
Figure 1. Observation sites in Beijing. All the data was obtained at BNU site except for gaseous pollutants, which were measured at Olympic Sports Center by National Environmental Bureau.
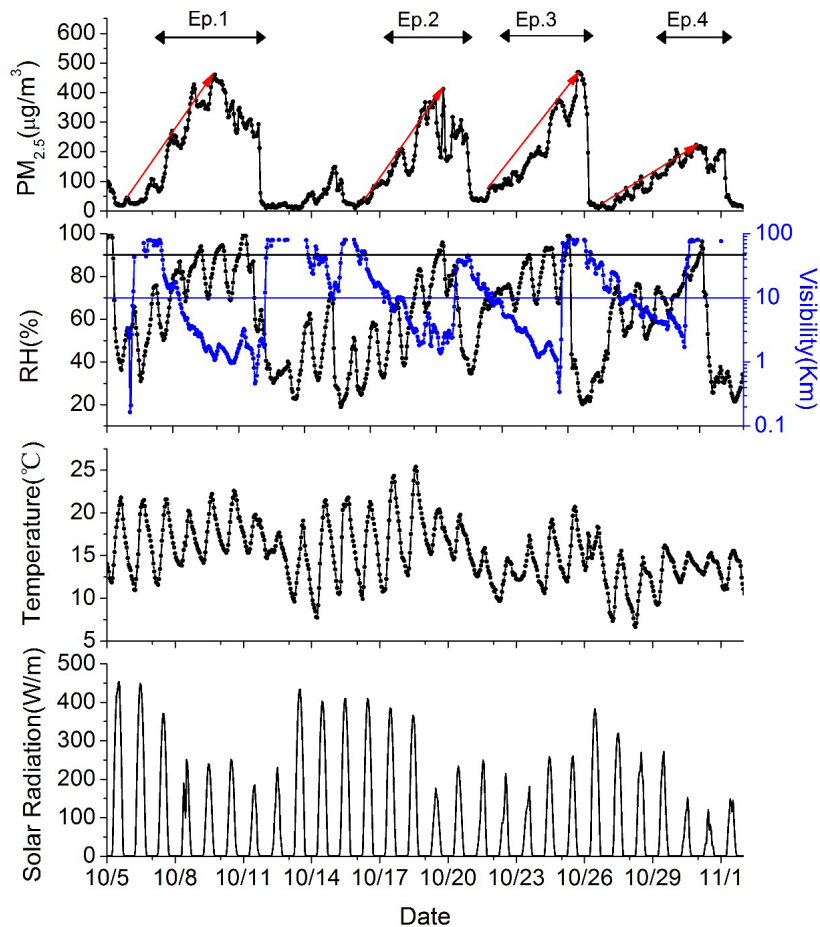
Figure 2. Time series of observed $PM_{2.5}$, RH, temperature and solar radiation in Beijing from 5 October to 2 November 2014.

Title Page

Abstract | Introduction

Conclusions | References

Tables | Figures

|◄ | ►|

◄ | ►

Back | Close

Full Screen / Esc

Printer-friendly Version

Interactive Discussion
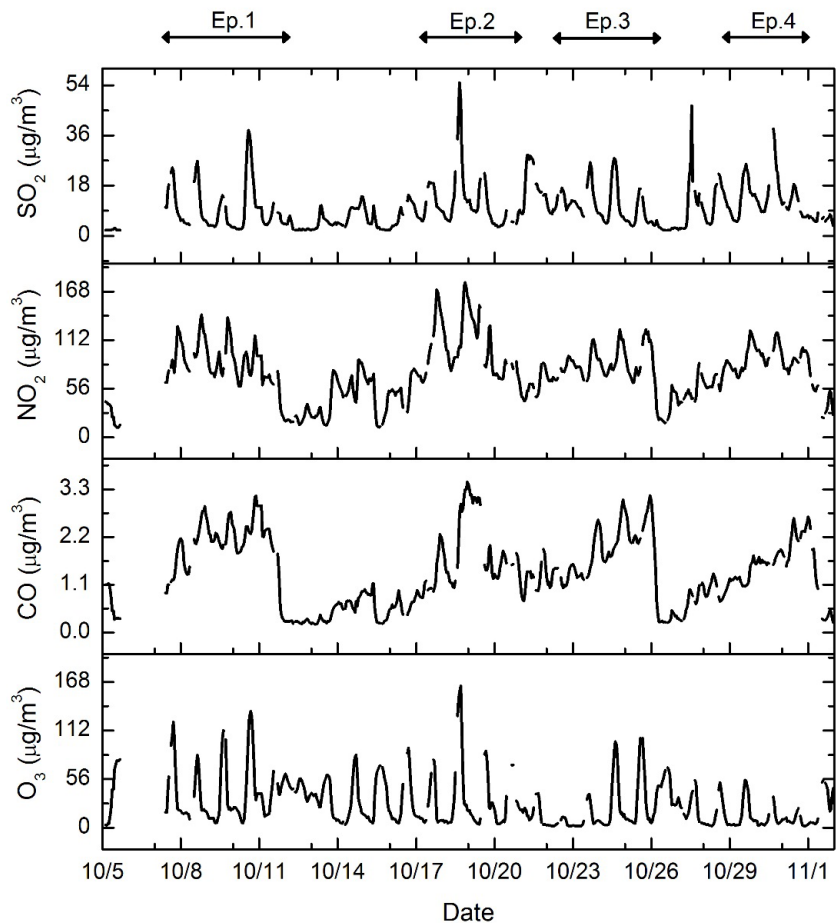
Figure 3. Time series of observed gaseous pollutants (SO_2, NO_2, CO, O_3) in Beijing from 5 October to 2 November 2014.
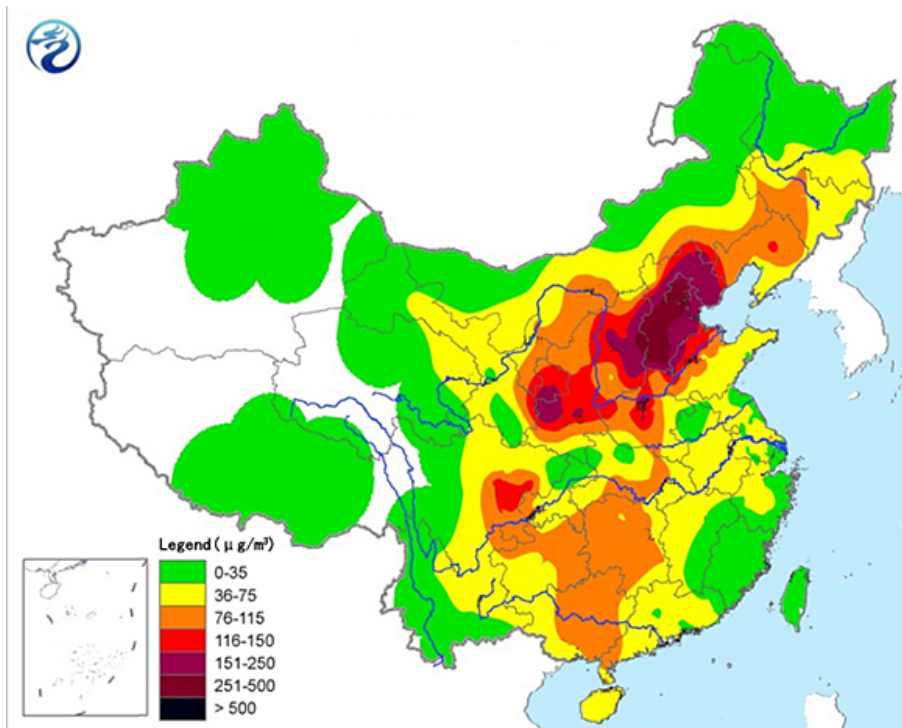
Figure 4. Spatial distribution of the $PM_{2.5}$ concentration over China from 5 a.m. 9 October to 5 a.m. 10 October (from China Meteorological Administration, http://www.nmc.gov.cn/publish/observations/environmental.htm).
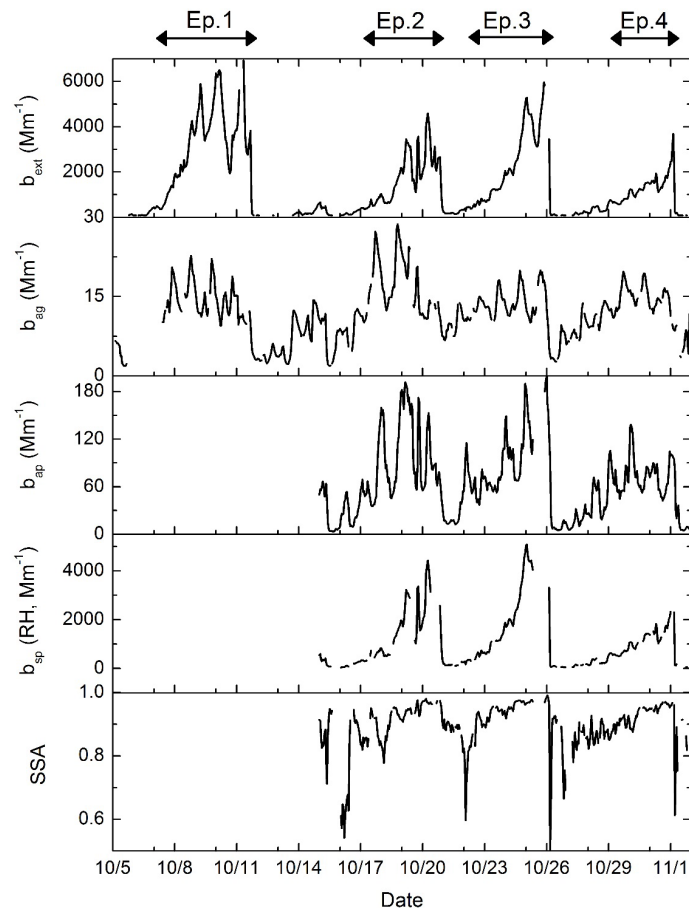
Figure 5. Time series of the atmospheric extinction coefficient b_{ext}, absorption by NO_2 coefficient b_{ag}, aerosol absorption coefficient b_{ap}, ambient aerosol scattering coefficient b_{sp}(RH), and single scattering albedo (SSA) in Beijing from 5 October to 2 November 2014.

Title Page

Abstract | Introduction

Conclusions | References

Tables | Figures

|◄ | ►|

◄ | ►

Back | Close

Full Screen / Esc

Printer-friendly Version

Interactive Discussion
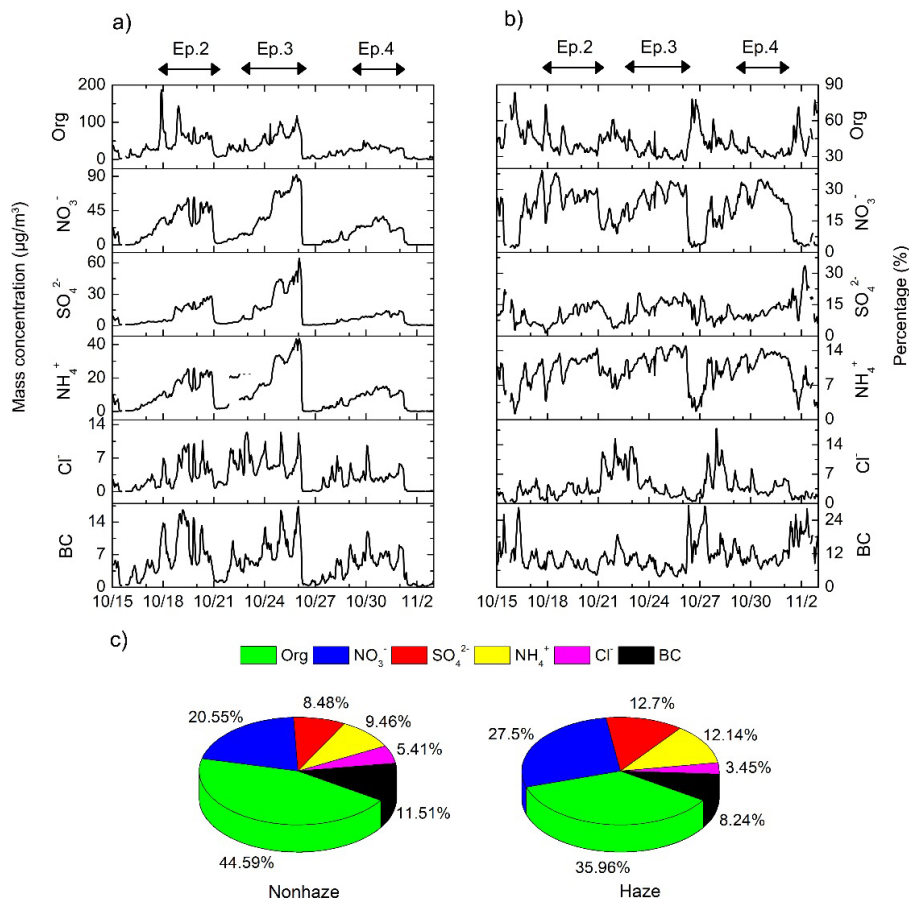
Figure 6. (a) Temporal variation of the mass concentration of each aerosol species in PM_1, **(b)** temporal variation of the mass fraction of each aerosol species in PM_1, **(c)** mass fraction of each aerosol species in PM_1 during non-haze and haze episodes from 15 October to 2 November 2014.
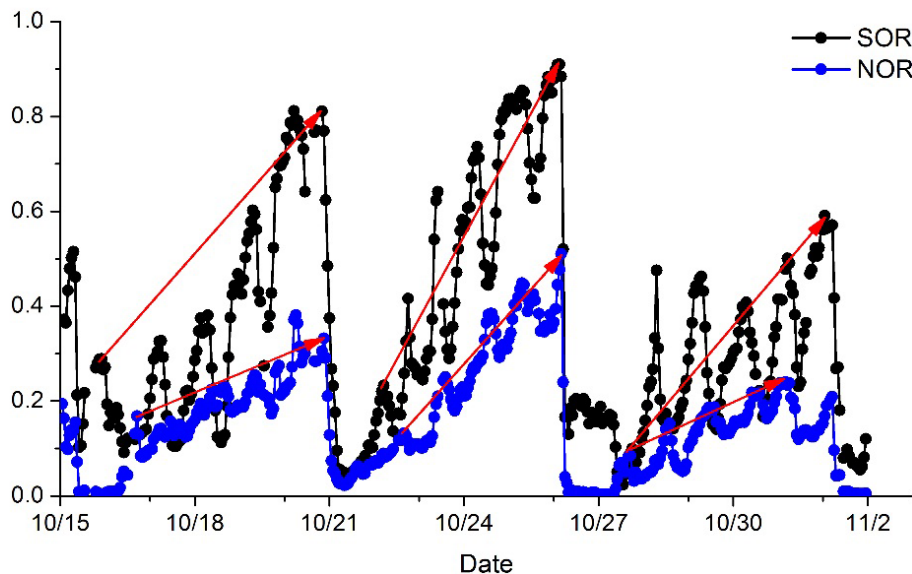
Figure 7. Time series of SOR (sulfate oxidation rate) and NOR (nitrate oxidation rate) from 15 October to 2 November 2014.
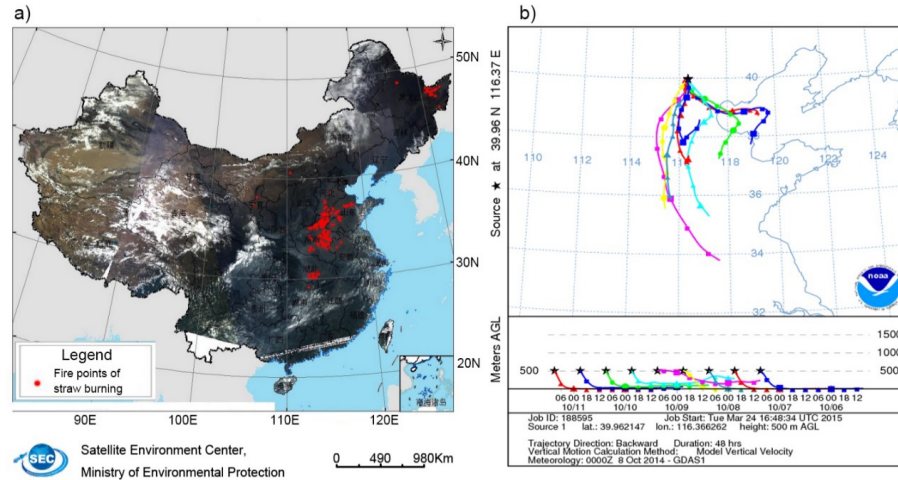
Figure 8. (a) Fire points of straw burning over China on 6 October 2014, **(b)** backward trajectories from Beijing for Episode 1.
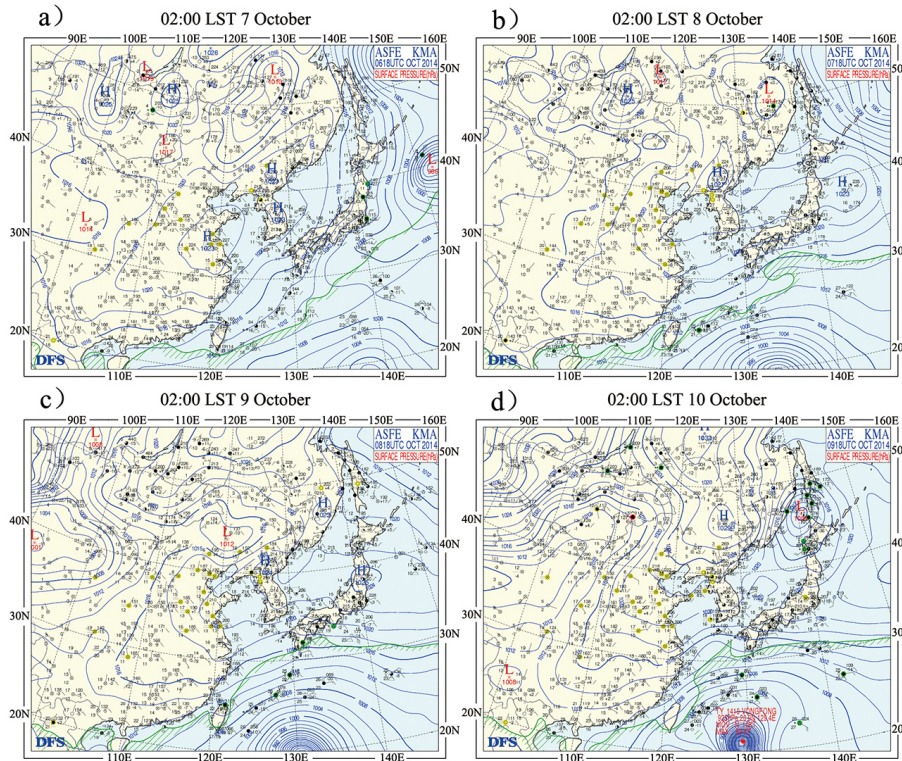
Figure 9. Surface pressure on the surface at **(a)** 02:00 LST, 7 October, **(b)** 02:00 LST, 8 October, **(c)** 02:00 LST, 9 October, and **(d)** 02:00 LST, 10 October.

Wind Vectors(KNTS) at Height: 10m AGL
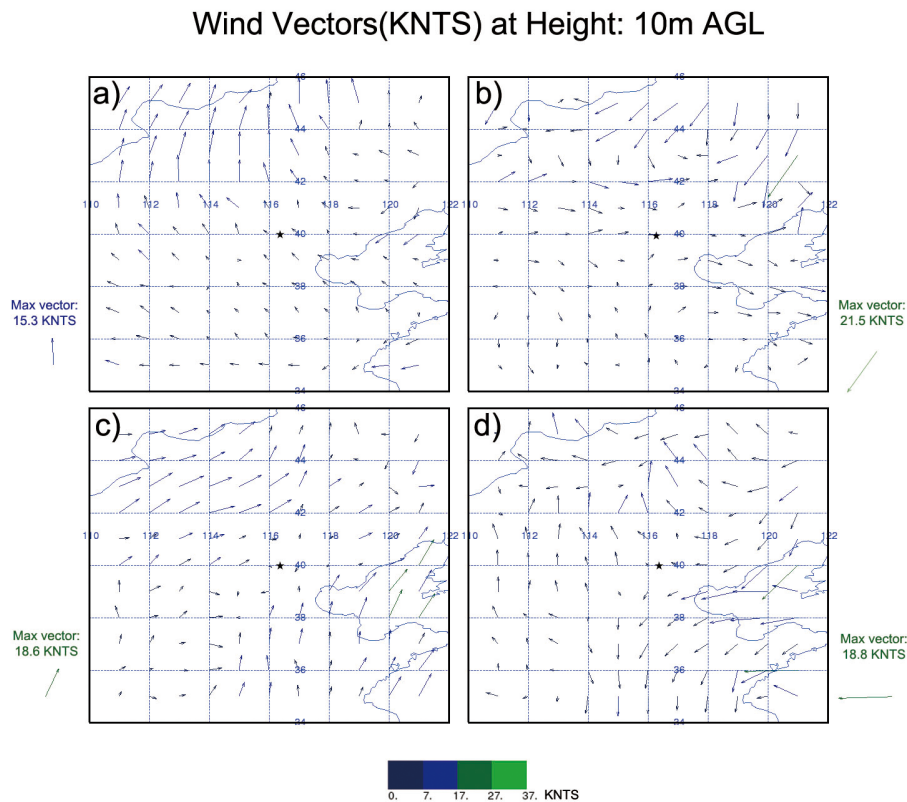
Figure 10. Wind field graphs of NCP at **(a)** 02:00, 10 October, **(b)** 02:00, 20 October, **(c)** 02:00, 24 October, and **(d)** 02:00 LST, 31 October; Black star denotes Beijing city, the color bar represents wind vectors.
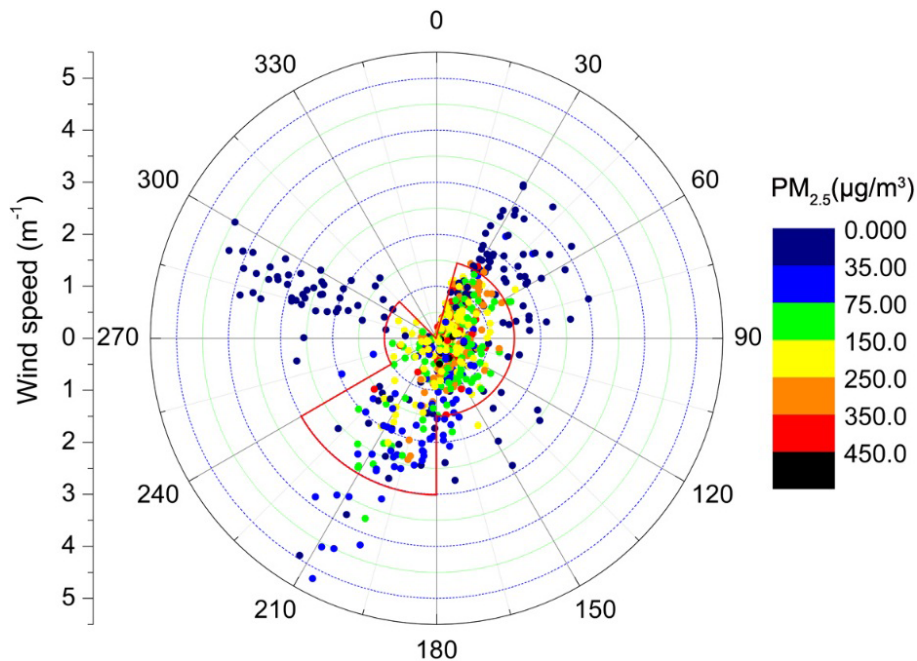
Figure 11. Wind rose diagrams of PM$_{2.5}$ in Beijing in October 2014.
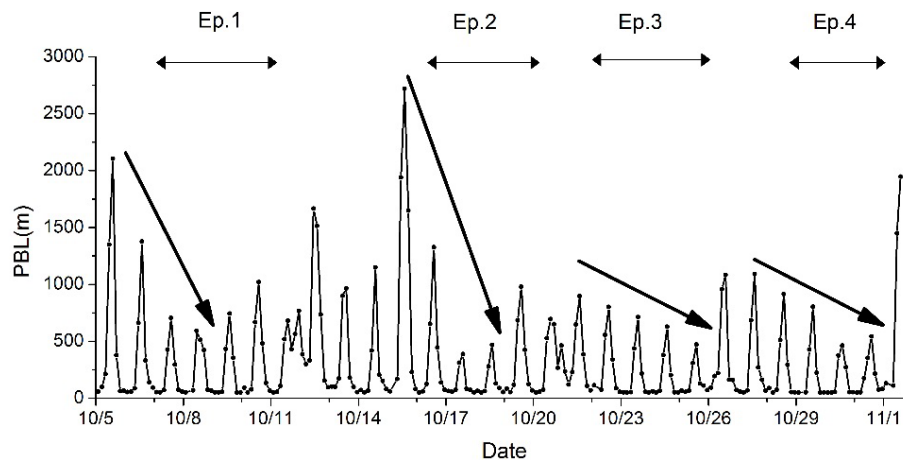
Figure 12. Time series of the PBL (planetary boundary layer) from 5 October to 2 November 2014.
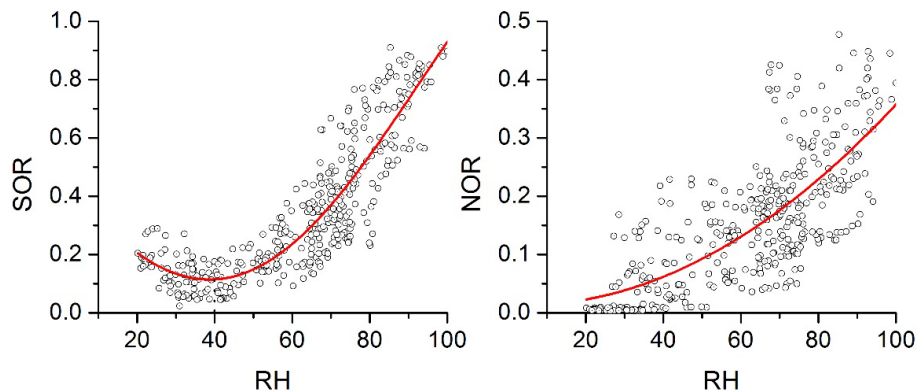
Figure 13. Relationship between RH (%) and SOR and between RH (%) and NOR during the haze episodes in October 2014.
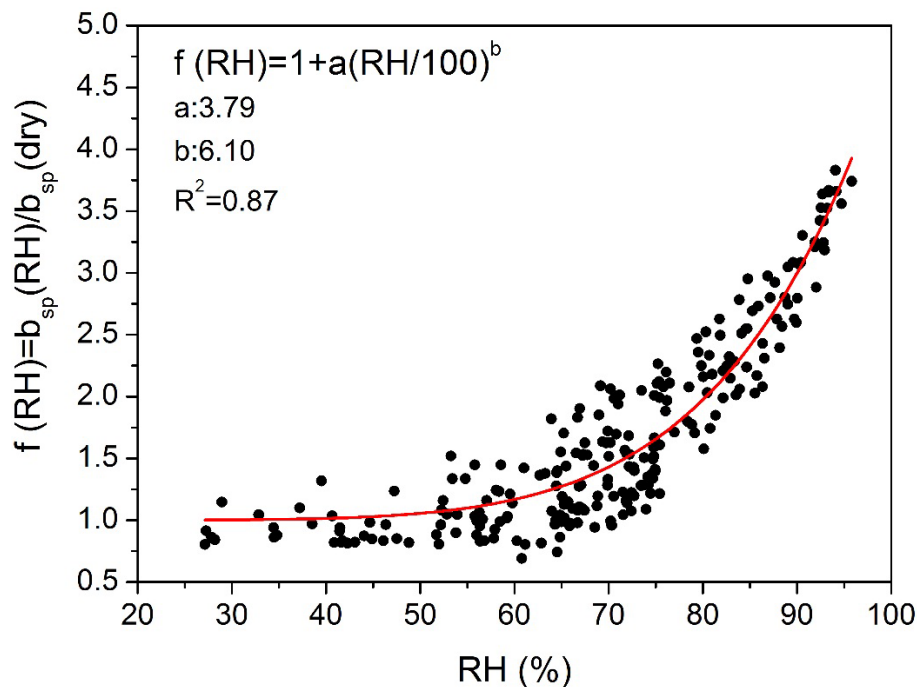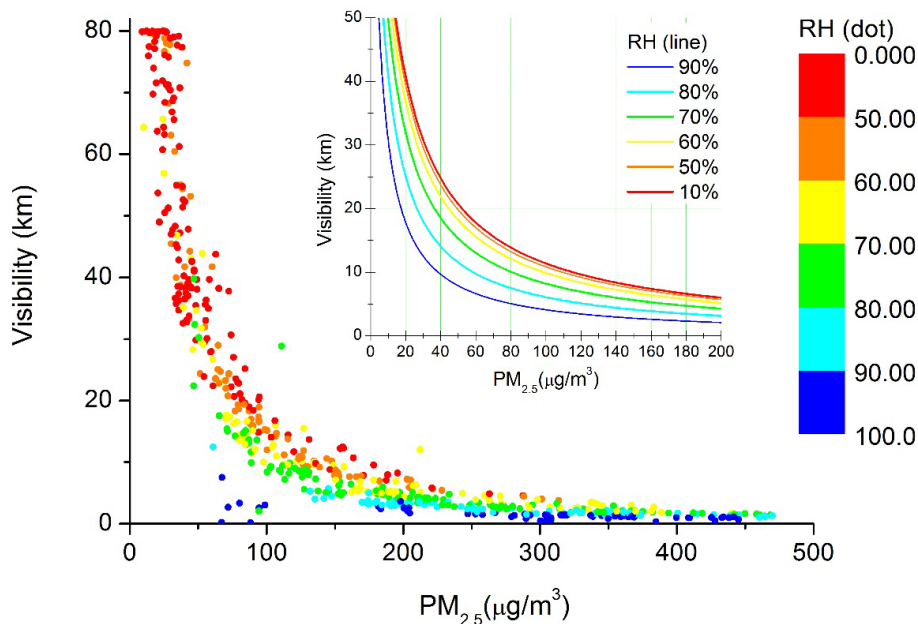
Figure 14. Hygroscopic growth for aerosol scattering $f(RH)$ as a function of RH with curve fitting. Scattered dots are the measured $f(RH)$ values, and the line is the empirical fitting curve.

Title Page

Abstract | Introduction

Conclusions | References

Tables | Figures

|◄ | ►|

◄ | ►

Back | Close

Full Screen / Esc

Printer-friendly Version

Interactive Discussion
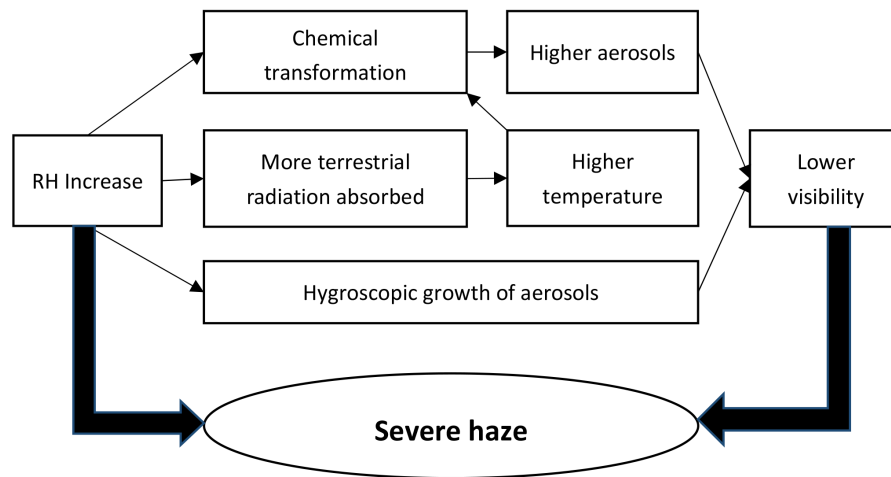
Figure 15. Variation of visibility at different RH values and different concentrations of PM$_{2.5}$, observed (dots) and simulated (lines).

Title Page

Abstract | Introduction

Conclusions | References

Tables | Figures

|◀ | ▶|

◀ | ▶

Back | Close

Full Screen / Esc

Printer-friendly Version

Interactive Discussion

Figure 16. The mechanism of how RH influenced haze formation.

Characteristics and formation mechanism of continuous extreme hazes

Y. Yang et al.

Title Page

Abstract	Introduction
Conclusions	References
Tables	Figures

|◄ | ►|

◄ | ►

Back | Close

Full Screen / Esc

Printer-friendly Version

Interactive Discussion